Single crystal synthesis and magnetic properties of a Shastry-Sutherland lattice compound BaNd$_2$ZnS$_5$

Brianna R. Billingsley,[1] Madalynn Marshall,[2] Zhixue Shu,[1] Huibo Cao,[2] and Tai Kong [1,3,*]

[1]*Department of Physics, University of Arizona, Tucson, Arizona 85721, USA*
[2]*Neutron Scattering Division, Oak Ridge National Laboratory, Oak Ridge, Tennessee 37831, USA*
[3]*Department of Chemistry and Biochemistry, University of Arizona, Tucson, Arizona 85721, USA*

Single crystals of a Shastry-Sutherland magnetic semiconductor, BaNd$_2$ZnS$_5$, were synthesized through a high-temperature solution growth technique. Physical properties were characterized by powder and single crystal x-ray diffraction, temperature- and field-dependent magnetization, and temperature-dependent specific heat measurements. BaNd$_2$ZnS$_5$ orders antiferromagnetically at 2.9 K, with magnetic moments primarily aligned within the *ab*-plane. Magnetic isothermal measurements show metamagnetic transitions at ∼15 kOe for the [110] direction and ∼21 kOe for the [100] direction. Estimated magnetic entropy suggests a double ground state for each neodymium ion.

I. INTRODUCTION

Geometrical frustration is one of the most effective ways to induce magnetic frustration in solids, which is commonly achieved by incorporating a triangular motif in the magnetic ion sublattice [1]. A Shastry-Sutherland lattice (SS) represents one of the geometrical frustrated lattice types. The original SS model considers competing magnetic interactions between a nearest-neighbor (NN) and an alternating next-nearest-neighbor (NNN) in a two-dimensional square lattice [2]. Depending on the relative ratio of the two magnetic interactions and spin number, different magnetic ground states were predicted, including long-range ordering and quantum spin liquid [2]. In real materials, to fulfill the required alternation of NNN interaction in the SS model, every other square unit needs to be distorted diagonally, essentially forming a pattern that is constructed by squares and triangles. Figure 1 illustrates an SS lattice, where J represents the NN interaction, also called the interdimer interaction, and J' represents the NNN interaction, also called the intradimer interaction. Materials will exhibit long-range magnetic ordering at a large J/J' and a dimer singlet state at a small J/J' [3,4]. The possibility of intermediate ground states, however, is under intensive theoretical investigation [5–14] and lacks sufficient experimental realization. The first example of an SS material is Sr Cu$_2$(BO$_3$)$_2$, where a gapped dimer singlet ground state was realized with a J/J' at ∼0.6 [3,15,16]. More materials were later demonstrated to host an SS lattice, with examples being metallic Gd$_2$Ge$_2$Mg [17], REB$_4$ [18–20], and RE_2Pt$_2$Pb [21] (RE = rare earth). Whereas a long-range RKKY-type interaction must be considered in a metallic compound, magnetism in a semiconducting or insulating SS lattice may involve simpler exchange interactions, and thus maps closer onto the

original SS model. As part of experimental exploration of different ground states of SS lattices, this study focuses on the single crystal study of a rare–earth-based semiconducting compound, BaNd$_2$ZnS$_5$.

The general chemical formula BaRE_2TMCh_5 (TM = transition metal, Ch = O, S) hosts many different materials [22–26]. For oxides, nearly the entire RE series is reported to exist when TM = Pd [22,27]. When TM = Zn or other $3d$ transition metals, the RE series will still form. However, the crystal structure changes from an SS lattice with a space group of *I4/mcm* for lighter REs, to an orthorhombic lattice with a space group of *Pbnm* for heavier RE elements, showing no SS lattice [28–30]. Such structural change sets up a limit on possible chemical tuning studies. The SS lattice can be restored for some heavier RE elements through high-pressure synthesis [31]. For sulfide, only the La-Nd versions are reported, with an *a*-axis constant of ∼7.9 Å and a *c*-axis constant of ∼13.6 Å. Both sulfide lattice constants are larger than the oxide version, which is consistent with ionic size differences between oxygen and sulfur [32]. BaNd$_2$ZnS$_5$ crystalizes in the *I4/mcm* space group (#140) with a Cs$_3$CoCl$_5$ structure type. A schematic crystal structure drawing of BaNd$_2$ZnS$_5$ is shown in Fig. 1. Neodymium atoms occupy a single atomic site in the crystal structure, which forms a planar SS lattice bridged by sulfur atoms [24]. Zinc also occupies only one atomic site, forming a square lattice in the *ab*-plane. Each SS layer is separated from each other with a layer of barium and transition metal, coordinated by sulfur. The magnetic SS layers are thus separated from each other by ∼6.8 Å. Within each SS plane, the long- and short-edge lengths in each triangular unit are about 4.154 Å (interdimer) and 3.596 Å (intradimer), respectively [24]. In addition to the difference in interneodymium distance, the Nd-S-Nd angle is different for inter- and intradimer. As shown in Fig. 1(b), the interdimer is channeled through three Nd-S-Nd links, each having an angle of ∼90°. The intradimer is channeled through four Nd-S-Nd
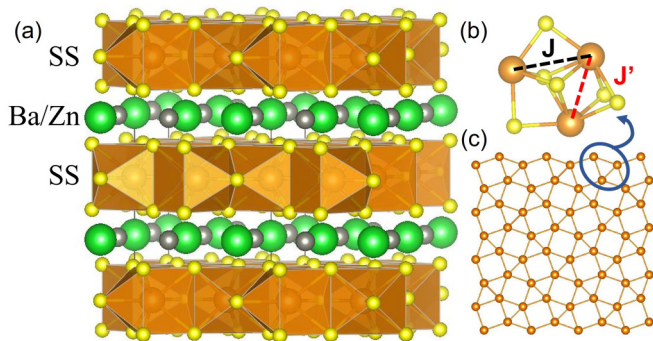
FIG. 1. (a) Schematic drawing of the crystal structure of BaNd$_2$ZnS$_5$. (b) Nd-S-Nd coordination for the selected triangular motif. (c) Neodymium sublattice in the *ab*-plane. Barium, zinc, neodymium, and sulfur atoms are represented by green, gray, brown, and yellow spheres, respectively.

FIG. 2. (a) Powder x-ray diffraction pattern for BaNdZnS$_5$. Top inset shows as-grown single crystals on a millimeter grid paper. (b) and (c) show diffraction peaks from certain lattice planes.

links, each having an angle of $\sim 72°$ [24]. For BaNd$_2$ZnO$_5$, the interdimer angle remains close to $90°$ while the intradimer angle is about $78°$ [33].

Previously, BaRE_2TMS$_5$ (RE = La−Nd, Sm; TM = Mn, Fe, Co, Zn) had only been synthesized in a powder form, where magnetic transition metals exhibit antiferromagnetic ordering at ~ 60 K, and magnetic rare-earth elements order at a much lower temperature below 5 K [24–26,34]. To study the magnetic behavior of the SS lattice, it is best to be free from other magnetic contributions. In this work, we focus on BaNd$_2$ZnS$_5$, where the transition metal site is occupied by nonmagnetic zinc. Measurements on the BaNd$_2$ZnS$_5$ powder sample suggest an insulating state with an activation energy of 1.46 eV, and an antiferromagnetic phase transition at 2.8 K [34]. Here we report the single crystal synthesis and detailed anisotropic magnetic properties of BaNd$_2$ZnS$_5$.

II. EXPERIMENTAL METHODS

BaNd$_2$ZnS$_5$ single crystals were synthesized using the high-temperature solution method [35]. The starting elements, comprised of barium pieces (Alfa Aesar, 99.2%), neodymium pieces (Alfa Aesar, 99.5%), zinc shot (Alfa Aesar, 99.999%), and sulfur pieces (Alfa Aesar, 99.999%), were packed into an alumina Canfield Crucible Set [36] with a molar ratio of Ba : Nd : Zn : S = 5 : 4 : 2 : 19, which was then sealed in a silica tube under vacuum. Air-sensitive barium and neodymium were handled in an argon glovebox. The ampoule was first heated to 430 °C over 3 hours, dwelled for 6 hours, then heated to 850 °C over 12 hours, where it dwelled for 5 hours, then finally heated to 1060 °C over 6 hours, and dwelled for 10 hours. After dwelling at 1060 °C, the ampoule was slowly cooled to 750 °C for decanting. The slow heating process is necessary to protect the alumina crucible from being attacked by barium and neodymium. Faster heating can result in a broken alumina crucible and silica ampoule. At 750 °C, significant sulfur vapor pressure is still present, as evidenced by a light-brown vapor found inside the silica tube. Dark-brown, cubic-like single crystals of BaNd$_2$ZnS$_5$ can be collected from the growth crucible. Typical crystals are shown in the Fig. 2 inset on millimeter grid paper.

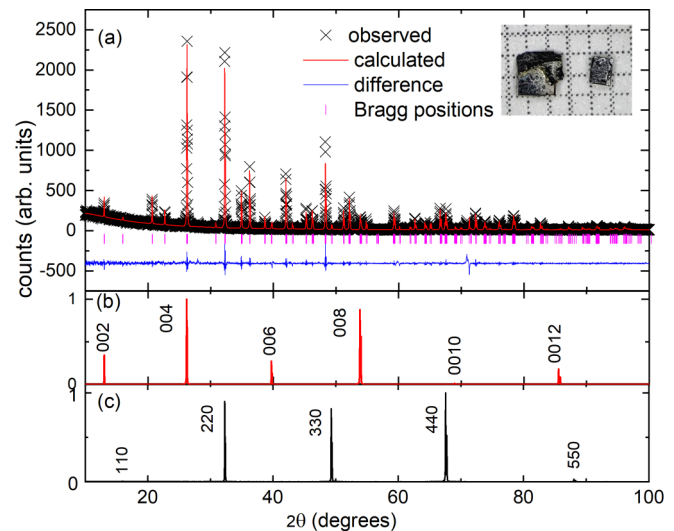Room-temperature powder x-ray diffraction (PXRD) was measured using a Bruker D8 Discover diffractometer, with a Cu Cu Kα radiation ($\lambda = 1.5406$ Å). A selection of single crystals was ground into powder and evenly spread on a vacuum-greased glass slide for measurement. PXRD data were analyzed using the General Structure Analysis System and the Le Bail method [37,38]. Crystalline orientation was determined by collecting single crystalline diffraction peaks using the powder diffractometer [39]. Single crystal x-ray diffraction (SXRD) measurements were carried out on a Rigaku XtaLAB PRO diffractometer using Mo K$_\alpha$ radiation, for a crystal of BaNd$_2$ZnS$_5$ at room temperature. Data collection and integrated were done using the Rigaku Oxford Diffraction CrysAlis Pro software [40], and the structural refinement was performed using a SHELXTL package [41]. The crystal structure was drawn using VESTA [42].

Anisotropic magnetization and specific heat data were measured using a quantum design physical property mea-

TABLE I. Room-temperature single crystal refinement information for BaNd$_2$ZnS$_5$.

Refined Formulag	BaNd$_2$ZnS$_5$
FW (g/mol)	651.49
Space group; Z	$I4/mcm$; 4
a (Å)	7.83402(16)
c (Å)	13.6071(4)
V(Å^3)	835.09(4)
Extinction coefficient	0.0141(4)
θ range (deg)	2.994–33.492
No. of reflections; R_{int}	12736; 0.0637
No. of independent reflections	455
No. of parameters	18
R_1; $\omega R_2(I > 2\delta(I))$	0.0174; 0.0401
Goodness of fit	1.181
Diffraction peak and hole (e$^-$/Å^3)	1.170, −1.370

TABLE II. Atomic coordinates for $BaNd_2ZnS_5$ including the equivalent isotropic displacement parameters.

Atom	Wyckoff	x	y	z	U_{eq}
Ba1	4a	0	0	¼	0.01247(12)
Nd1	8h	0.16230(2)	0.66230(2)	0	0.00902(11)
Zn1	4b	0	½	¼	0.01056(16)
S1	4c	0	0	0	0.0112(3)
S2	16l	0.65013(7)	0.15013(7)	0.13405(7)	0.01192(17)

surement system (Dynacool; 1.8 to 300 K, 0 to 90 kOe). Magnetization was measured using the vibrating sample magnetometer function. Single crystalline samples were manually mounted on a silica sample holder in preferred orientation with GE varnish. Zero-field specific heat data were measured down to 1.8 K using the two-tau relaxation method. The specific heat of a $BaLa_2ZnS_5$ single crystal was also measured to serve as the nonmagnetic lattice contribution for the estimation of magnetic entropy in $BaNd_2ZnS_5$.

III. RESULTS AND DISCUSSION

PXRD data shown in Fig. 2 are in good agreement with reported crystal structure of $BaNd_2ZnS_5$ [24]. Nonmagnetic Ba-S binary impurity phases can sometimes be found on the surface of single crystals, which can be mechanically removed. Facets of as-grown single crystals can be indexed by either (00l) or (hh0). A selection of observed single crystal diffraction peaks is shown in the lower panels of Fig. 2. Because $BaNd_2ZnS_5$ has a tetragonal crystal structure, [100] was aligned by a 45° in-plane rotation away from the [110] direction. The room-temperature SXRD result is consistent with previously reported powder refinement results [24]. All atomic sites are fully occupied. Detailed crystal structure refinement results are listed in Tables I–III. Recent neutron scattering data on $BaNd_2ZnO_5$ [33] and $BaNd_2ZnS_5$ [43] suggest that neodymium local magnetic moments prefer to align along [110] or the equivalent direction [1−1 0], breaking the in-plane magnetic isotropy. In terms of crystal structure, anisotropic displacement parameters listed in Table III show a small displacement anisotropy of neodymium ions at room temperature, which shows the symmetry similarity with its in-plane magnetic anisotropy at low temperatures. Such coincidence may worth further investigation.

Figure 3 shows the anisotropic, temperature-dependent magnetization of $BaNd_2ZnS_5$ measured at 10 kOe. The polycrystalline averaged magnetization was calculated via $\chi_{poly} = 1/3\chi_{001} + 1/3\chi_{100} + 1/3\chi_{110}$. Here, χ is defined as M/H.
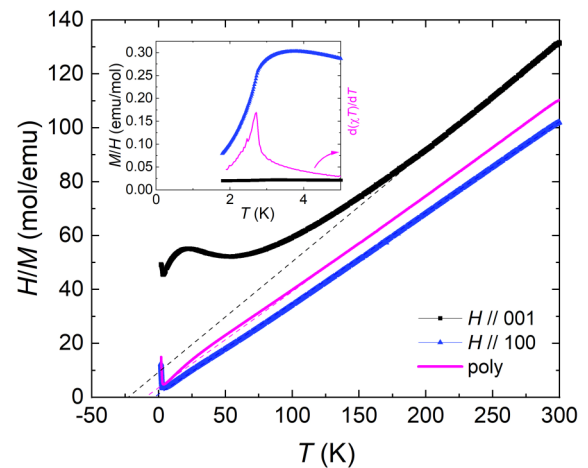

FIG. 3. Anisotropic, temperature-dependent inverse magnetization of $BaNd_2ZnS_5$. The dashed lines represent high-temperature Curie-Weiss fits. The inset shows a zoom-in view of magnetization at low temperatures and $d\chi T/dT$ in arbitrary units.

At high temperatures, the magnetization is anisotropic with $\chi_{ab} > \chi_c$, which is likely due to the crystal electric field (CEF) effect that is commonly seen in rare-earth–based compounds [44,45]. The inverse magnetic susceptibility of the polycrystalline averaged data remains linear down to low temperatures even in the presence of CEF splitting [46]. In-plane magnetic anisotropy is weak at 10 kOe, and thus only χ_{100} is displayed. A Curie-Weiss fit ($\chi = C/(T-\theta)$) to the high-temperature χ_{poly} data gives an effective moment of 3.3 μ_B/Nd, close to the theoretical value of 3.62 μ_B/Nd. Anisotropic Curie-Weiss temperatures are $\theta_{poly} = -8$ K, $\theta_{ab} = -1$ K, $\theta_c = -21$ K, indicating primarily antiferromagnetic interactions. At low temperatures, a clear drop in magnetization indicates an antiferromagnetic ordering. Taking the peak in $d(\chi T)/dT$ [47] as a criteria, the magnetic ordering temperature is determined as ∼2.7 K.

Metamagnetic transitions were observed below the antiferromagnetic ordering temperature. Figure 4 shows anisotropic magnetic isotherm measurements at 1.8 K. Along the c-axis ([001] direction), the magnetization increases linearly with the applied magnetic field up to 90 kOe. For in-plane orientations, the metamagnetic transition appears at ∼15 kOe for the [110] direction and at ∼21 kOe for the [100] direction. The metamagnetic transition fields were determined by the peak fields in dM/dH curves. The ratio of the metamagnetic phase transition fields between the two in-plane orientations is close to $\sqrt{2}$, indicating that an equivalent 15-kOe magnetic field along [110] is needed to induce the metamagnetic phase. This is

TABLE III. Anisotropic displacement parameters for each atomic site in $BaNd_2ZnS_5$.

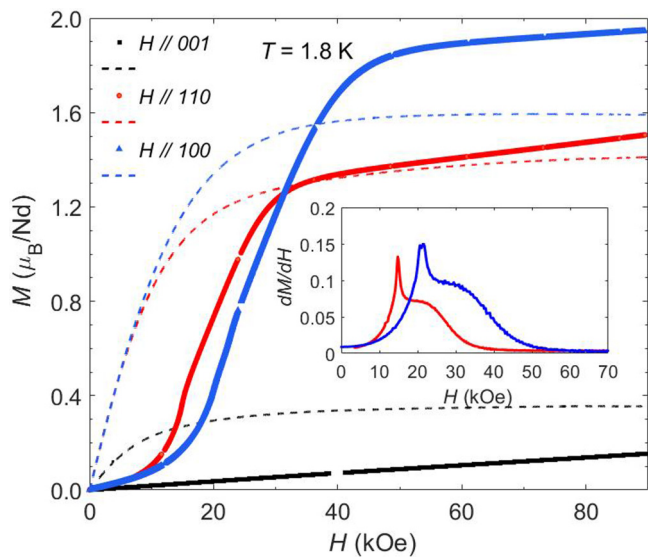| Atom	U11	U22	U33	U23	U13	U12
Ba1	0.01218(14)	0.01218(14)	0.01305(19)	0	0	0
Nd1	0.00873(12)	0.00873(12)	0.00959(15)	0	0	–0.00124(6)
Zn1	0.0120(2)	0.0120(2)	0.0077(3)	0	0	0
S1	0.0093(4)	0.0093(4)	0.0149(7)	0	0	0
S2	0.0125(2)	0.0125(2)	0.0107(4)	0.00212(18)	0.00212(18)	–0.0015(2)

FIG. 4. Anisotropic magnetic isotherms of BaNd$_2$ZnS$_5$ measured at 1.8 K. The solid lines represent data from pure BaNd$_2$ZnS$_5$. The dashed lines represent data from a diluted sample, BaLa$_{1.86}$Nd$_{0.14}$ZnS$_5$, as detailed in the text. The inset shows the dM/dH as a function of applied magnetic field up to 70 kOe.

FIG. 5. Zero-field, temperature-dependent specific heat of BaNd$_2$ZnS$_5$. The left inset shows the estimated magnetic entropy. The right inset shows the high-temperature magnetic specific heat with the calculated Schottky anomaly contrition (magenta dotted line) as detailed in the text. The red solid line shows the specific heat of BaLa$_2$ZnS$_5$.

consistent with the recent neutron scattering result, indicating magnetic moments are along [110] and equivalent directions [43]. Kinks in magnetization appear at ~ 0.35 μ_B/Nd for [110] and at ~ 0.51 μ_B/Nd for [100]. Because 1.8 K is close to the magnetic ordering temperature, it is possible that these magnetization kinks may appear more plateau-like at lower temperatures, similar to other SS lattice compounds. Note that the dM/dH curve for [100] (Fig. 4 inset) has a relatively rounded peak shape compared to that along [110], which may suggest the existence of a small magnetization plateau. The magnetization for both in-plane orientations appears to be saturating at a high magnetic field. Extrapolating the linear magnetization curve above 60 kOe back to the zero field gives a moment size of ~ 1.2 μ_B for [110] and ~ 1.8 μ_B for [100]. Such in-plane magnetic anisotropy likely result from a combined influence of CEF effect and applied magnetic field [48]. The anisotropic magnetization data on diluted BaLa$_{1.86}$Nd$_{0.14}$ZnS$_5$ single crystals are shown by dashed lines in Fig. 4. The doping ratio was measured by scanning electron microscopy. The single ion results obtained on the diluted
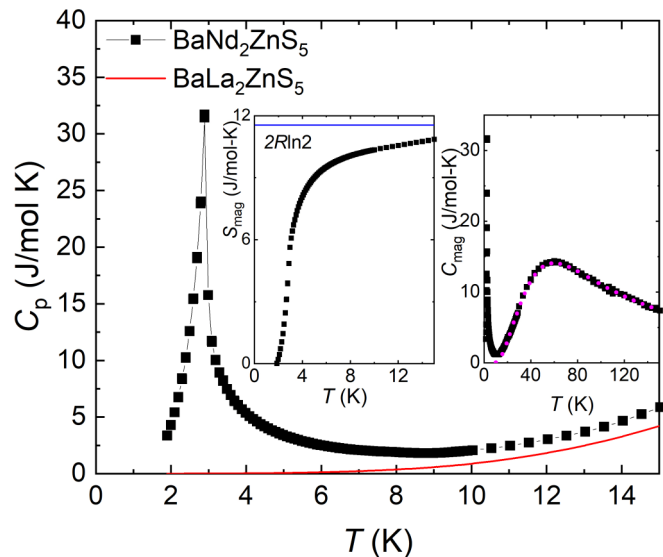
sample also show an in-plane magnetic anisotropy at high magnetic fields, which accounts for only part of the observed magnetic anisotropy in the pure BaNd$_2$ZnS$_5$. Additional in-plane anisotropy in pure BaNd$_2$ZnS$_5$ may come from a change in CEF scheme due to a strong mean field in the magnetically ordered state.

Figure 5 shows the zero-field specific heat (C_p) data of BaNd$_2$ZnS$_5$. A λ-shaped peak suggests a second-order phase transition at 2.9 K, which is consistent with the antiferromagnetic ordering observed in the magnetization data and in a previous report [34]. Magnetic specific heat (C_{mag}) can be estimated by subtracting the C_p of BaLa$_2$ZnS$_5$ as the lattice contribution, as shown by the red solid line in Fig. 5. The magnetic entropy of BaNd$_2$ZnS$_5$ reaches close to Rln2 per neodymium ion above 10 K, which indicates a doublet CEF ground state of neodymium in BaNd$_2$ZnS$_5$. At high temperatures, a broad dome in C_{mag} centered around 60 K is likely a Schottky anomaly due to CEF excitation. Because Nd^{3+} is a Kramer's ion, C_{mag} can be fitted with five-doublets Schottky excitation as

$$C_{mag} = \frac{2R}{T^2} \frac{\left(\sum_{i=2}^{i=5} \varepsilon_i^2 e^{-\varepsilon_i/T}\right)\left(1 + \sum_{i=2}^{i=5} e^{-\varepsilon_i/T}\right) - \left(\sum_{i=2}^{i=5} \varepsilon_i e^{-\varepsilon_i/T}\right)^2}{\left(1 + \sum_{i=2}^{i=5} e^{-\varepsilon_i/T}\right)^2}.$$

Here, ε_i is the energy of each CEF doublet in the unit of kelvin, R is the natural gas constant, T is temperature, and the prefactor 2 comes from two neodymium ions per formula unit. The ground state ε_1 is assumed to be zero. The fitted curve is shown by the dotted magenta line in the right inset of Fig. 5. The broad dome around 60 K is mostly due to

a first excited state at $\varepsilon_2 \sim 97$ K and two close-by doublets $\varepsilon_3 = \varepsilon_4 \sim 205$ K. Another doublet may situate at higher energies at $\varepsilon_5 \sim 480$ K. Better estimation on higher lying CEF levels will require C_{mag} data at higher temperatures. Compared to the previous polycrystalline report [34], where only one doublet was fitted at 197 K, the current estimation of two

close-by doublets at $\sim$200 K is closer to the scenario found in $BaNd_2ZnO_5$, where three doublets were reported to exist within 5 meV. A more detailed CEF-level determination via inelastic neutron scattering will be published elsewhere.

The fractional magnetization plateau in the SS model is of great theoretical interest. Considering magnetic coupling beyond the original NN and NNN interaction can bring in additional fractions other than the commonly predicted 1/3 M_{sat} for two dimensions [5]. Whereas most models consider Ising spin, the current planar magnetization would be more suitably described using an XY model. The planar magnetic anisotropy also posts difficulty in defining the fraction of magnetization plateau at the metamagnetic transition because the size of the local moment originates from the interplay between CEF-level hybridization and applied magnetic field [48]. Using the magnetization values shown in Fig. 4, the metamagnetic phase at $\sim$20 kOe roughly corresponds to 1/3 to 1/4 of the saturation value for each in-plane orientation.

The physical properties of $BaNd_2ZnS_5$ are similar to that of recently reported $BaNd_2ZnO_5$ [33,49], which orders antiferromagnetically at a lower temperature of 1.65 K. Given that the Nd-Nd distance in $BaNd_2ZnS_5$ is longer by $\sim$3.5% for intradimer and $\sim$18% for interdimer compared to $BaNd_2ZnO_5$, thus reducing dipole-dipole interaction, sulfur bridging atoms may be facilitating a stronger Nd-Nd interaction than oxygen atoms. Continuing the current trend in crystal structure, replacing sulfur with larger chalcogen atoms such as selenium will further expand the lattice. Additionally, the ratio between intradimer and interdimer distance may continue to decrease, thus favoring the formation of a singlet dimer ground state if an antiferromagnetic exchange interaction is considered [7]. The CEF ground state is also a doublet in $BaNd_2ZnO_5$ with an ordered moment of 1.9 μ_B. This is comparable to the current observed saturation moment of $\sim$1.8 μ_B for $BaNd_2ZnS_5$. A zero-field neutron scattering measurement on $BaNd_2ZnO_5$ and $BaNd_2ZnS_5$ revealed an antiferromagnetic structure with in-plane, orthogonally arranged ferromagnetic dimers [33,43]. This is similar to the theoretical picture of a Neel state [7], except without catching the orthogonal arrangement of the ferromagnetic dimers. The difference between experimental and theoretical magnetic structure is perhaps related to the planar magnetic anisotropy in both $BaNd_2ZnO_5$ and $BaNd_2ZnS_5$. Although a weak metamagnetic transition feature was observed in the $BaNd_2ZnO_5$ powder sample [49], no neutron data were available to investigate the corresponding magnetic structure in the metamagnetic state. Since magnetic field is known to introduce different magnetic structures in SS compounds [5,50], more detailed neutron scattering at various

applied fields will be necessary to gain physical insights into this family of compounds in the future.

Compared to copper in $SrCu_2(BO_3)_2$, where the gapped dimer singlet ground state is explained by a spin ½ Heisenberg model [3], neodymium in $BaNd_2ZnS_5$ has an antiferromagnetic ground state with a larger and anisotropic local spin. Although $BaNd_2ZnO_5$ and $BaNd_2ZnS_5$, having different $J/J\prime$, both end up in an antiferromagnetic ground state, the BaRE2ZnCh5 family of compounds offers more tunability in exploring the phase space of the two-dimensional SS model. Such tunability can be achieved through varying local spin properties by using different rare-earth elements and controlling the $J/J\prime$ ratio by using different chalcogen atoms. Moreover, the relative weak interactions in the rare-earth family significantly reduce the required field to reach those possible plateau phases, i.e., lower the access barrier for many techniques, including neutron scattering. It is thus of great interest to investigate systematically the magnetic properties of BaRE_2ZnCh_5.

IV. CONCLUSION

We have reported the single crystal growth and anisotropic magnetic characterization of the SS lattice compound. Millimeter-sized single crystals can be obtained through a high-temperature solution growth technique. Single crystal structural refinement is consistent with a previous powder sample result. The refined anisotropic displacement parameters suggest a small in-plane anisotropy of the neodymium ions at room temperature. At high temperatures, $BaNd_2ZnS_5$ is paramagnetic with a large magnetic anisotropy. Local magnetic moments are primarily lying in-plane. A long-range antiferromagnetic ordering is observed at 2.9 K, below which metamagnetic transitions were observed for in-plane [100] and [110] directions. Specific heat measurements show a doublet ground state and a Schottky-like anomaly due to higher lying CEF levels.

[1] A. P. Ramirez, Annu. Rev. Mater. Sci. **24**, 453 (1994).

[2] B. S. Shastry and B. Sutherland, Phys. B **108**, 1069 (1981).

[3] S. Miyahara and K. Ueda, J. Phys. Condens. Matter **15**, R327 (2003).

[4] A. Vasiliev, O. Volkova, E. Zvereva, and M. Markina, npj Quantum Mater. **3**, 18 (2018).

[5] Y. I. Dublenych, Phys. Rev. Lett. **109**, 167202 (2012).

[6] M. Al Hajj and J.-P. Malrieu, Phys. Rev. B **72**, 094436 (2005).

[7] A. Koga, N. Kawakami, and M. Sigrist, J. Phys. Soc. Jpn **72**, 938 (2002).

[8] W. Zheng, J. Oitmaa, and C. J. Hamer, Phys. Rev. B **65**, 014408 (2001).

[9] R. Darradi, J. Richter, and D. J. J. Farnell, Phys. Rev. B **72**, 104425 (2005).

[10] P. Corboz and F. Mila, Phys. Rev. B **87**, 115144 (2013).

[11] A. Läuchli, S. Wessel, and M. Sigrist, Phys. Rev. B **66**, 014401 (2002).

[12] D. C. Ronquillo and M. R. Peterson, Phys. Rev. B **90**, 201108(R) (2014).

[13] M. Malki and G. S. Uhrig, Phys. Rev. B **99**, 174412 (2019).

[14] V. Dwivedi, C. Hickey, T. Eschmann, and S. Trebst, Phys. Rev. B **98**, 054432 (2018).

[15] H. Kageyama, K. Yoshimura, R. Stern, N. V. Mushnikov, K. Onizuka, M. Kato, K. Kosuge, C. P. Slichter, T. Goto, and Y. Ueda, Phys. Rev. Lett. **82**, 3168 (1999).

[16] S. Miyahara and K. Ueda, Phys. Rev. Lett. **82**, 3701 (1999).

[17] W. Choe, G. J. Miller, and E. M. Levin, J. Alloys Compd. **329**, 121 (2001).

[18] Z. Fisk, M. B. Maple, D. C. Johnston, and L. D. Woolf, Solid State Commun. **39**, 1189 (1981).

[19] F. Iga, A. Shigekawa, Y. Hasegawa, S. Michimura, T. Takabatake, S. Yoshii, T. Yamamoto, M. Hagiwara, and K. Kindo, J. Magn. Magn. Mater. **310**, e443 (2007).

[20] S. S. Sunku, T. Kong, T. Ito, P. C. Canfield, B. S. Shastry, P. Sengupta, and C. Panagopoulos, Phys. Rev. B **93**, 174408 (2016).

[21] G. Melnyk, L. D. Gulay, and W. Tremel, J. Alloys Compd. **528**, 70 (2012).

[22] T. Taniguchi, Y. Kawaji, T. C. Ozawa, Y. Nagata, Y. Noro, H. Samata, and M. D. Lan, J. Alloys Compd. **386**, 63 (2005).

[23] T. C. Ozawa, T. Taniguchi, Y. Kawaji, S. Mizusaki, Y. Nagata, Y. Noro, H. Samata, H. Mitamura, and S. Takayanagi, J. Alloys Compd. **448**, 96 (2008).

[24] M. Wakeshima and Y. Hinatsu, J. Solid State Chem. **159**, 163 (2001).

[25] K. Ino, M. Wakeshima, and Y. Hinatsu, Mater. Res. Bull. **36**, 2207 (2001).

[26] M. Wakeshima and Y. Hinatsu, J. Solid State Chem. **153**, 330 (2000).

[27] H. Müller-Buschbaum and L. Wulff, Z. Naturforsch. B **51**, 461 (1996).

[28] J. A. Kaduk, W. Wong-Ng, W. Greenwood, J. Dillingham, and B. H. Toby, J. Res. Natl. Inst. Stand. Technol **104**, 147 (1999).

[29] W. Wong-Ng, B. Toby, and W. Greenwood, Powder Diffr. **13**, 144 (1998).

[30] H. Müller-Buschbaum and S. Möhr, J. Less Common Met. **170**, 127 (1991).

[31] Y. Ishii, J. Chen, H. K. Yoshida, M. Oda, A. D. Christianson, and K. Yamaura, J. Solid State Chem. **289**, 121489 (2020).

[32] R. D. Shannon, Acta Crystallogr. Sect. A **32**, 751 (1976).

[33] Y. Ishii, G. Sala, M. B. Stone, V. O. Garlea, S. Calder, J. Chen, H. K. Yoshida, S. Fukuoka, J. Yan, C. dela Cruz, M.- H. Du, D. S. Parker, H. Zhang, C. D. Batista, K. Yamaura, and A. D. Christianson, Phys. Rev. Mater. **5**, 064418 (2021).

[34] M. Wakeshima, N. Taira, Y. Hinatsu, A. Tobo, K. Ohoyama, and Y. Yamaguchi, J. Solid State Chem. **174**, 159 (2003).

[35] P. C. Canfield and Z. Fisk, Philos. Mag. B **65**, 1117 (1992).

[36] P. C. Canfield, T. Kong, U. S. Kaluarachchi, and N. H. Jo, Philos. Mag. **96**, 84 (2016).

[37] B. H. Toby, J. Appl. Crystallogr. **34**, 210 (2001).

[38] A. C. Larson and R. B. Von Dreele, General Structure Analysis System (GSAS), Report number LAUR 86-748, Los Alamos National Laboratory, 2000.

[39] A. Jesche, M. Fix, A. Kreyssig, W. R. Meier, and P. C. Canfield, Philos. Mag. **96**, 2115 (2016).

[40] Rigaku, CrysAlisPro Software System, Version 1.171.41.93a. (2020).

[41] G. M. Sheldrick, Acta Cryst. **C71**, 3 (2015).

[42] G. M. Sheldrick, Acta Cryst. **A71**, 3 (2015).

[43] M. Marshall, B. R. Billingsley, X. Bai, T. Kong, and H. Cao, arXiv:2208.02795.

[44] S. L. Bud'ko, Z. Islam, T. A. Wiener, I. R. Fisher, A. H. Lacerda, and P. C. Canfield, J. Magn. Magn. Mater. **205**, 53 (1999).

[45] T. Kong, C. E. Cunningham, V. Taufour, S. L. Bud'ko, M. L. C. Buffon, X. Lin, H. Emmons, and P. C. Canfield, J. Magn. Magn. Mater. **358–359**, 212 (2014).

[46] B. D. Dunlap, J. Magn. Magn. Mater. **37**, 211 (1983).

[47] M. E. Fisher, Philos. Mag. **7**, 1731 (1962).

[48] T. Kong, W. R. Meier, Q. Lin, S. M. Saunders, S. L. Bud'ko, R. Flint, and P. C. Canfield, Phys. Rev. B **94**, 144434 (2016).

[49] H. Kageyama, Y. Ueda, Y. Narumi, K. Kindo, M. Kosaka, and Y. Uwatoko, Prog. Theor. Phys. Suppl. **145**, 17 (2002).

[50] Z. Y. Meng and S. Wessel, Phys. Rev. B **78**, 224416 (2008).